

# Discovery of state transition behaviors in PSR J1124–5916

M. Y. Ge<sup>1</sup>, J. P. Yuan<sup>2,3</sup>, F. J. Lu<sup>1</sup>, H. Tong<sup>4</sup>, S. Q. Zhou<sup>5</sup>, L. L. Yan<sup>6</sup>, L. J. Wang<sup>1</sup>, Y. L. Tuo<sup>1,7</sup>, X. F. Li<sup>1</sup>, L. M. Song<sup>1,7</sup>

<sup>1</sup> *Key Laboratory of Particle Astrophysics, Institute of High Energy Physics, Chinese Academy of Sciences, Beijing 100049, China. Email: gemy@ihep.ac.cn*

<sup>2</sup> *Xinjiang Astronomical Observatory, Chinese Academy of Sciences, Xinjiang 830011, China*

<sup>3</sup> *Center for Astronomical Mega-Science, Chinese Academy of Sciences, Beijing, 100012, China*

<sup>4</sup> *School of Physics and Electronic Engineering, Guangzhou University, Guangzhou 510006, China*

<sup>5</sup> *China West Normal University, Sichuan 637002, China*

<sup>6</sup> *School of Mathematics and Physics, Anhui Jianzhu University, Hefei 230601, China*

<sup>7</sup> *University of Chinese Academy of Sciences, Chinese Academy of Sciences, Beijing 100049, China*

## ABSTRACT

With the twelve-year long observations by *Fermi*-LAT, we discover two pairs of spin-down state transitions of PSR J1124–5916, making it the second young pulsar detected to have such behaviors. PSR J1124–5916 shows mainly two states according to its spin-down rate evolution, the normal spin-down state and the low spin-down state. In about 80% of the observation time, the pulsar is in the normal spin-down state, in which the spin-down rate decreases linearly and gives a braking index of  $1.98 \pm 0.04$ . The two transitions to the low spin-down state are in MJD 55183–55803 and MJD 56114–56398 respectively, with fractional amplitudes both  $\sim 0.4\%$ . No significant difference between the  $\gamma$ -ray profiles of the two spin-down states is detected, which is similar to PSR B0540-69, the other young pulsar with state transition detected.

*Subject headings:* glitch — stars: neutron — pulsars: general — X-rays: individual (PSR J1124–5916)

## 1. Introduction

The rotation evolution of a pulsar reflects the properties of its magnetosphere. For pulsars, the rotation frequency  $\nu$  decreases with time and this slow-down is usually described by the relation  $\dot{\nu} = -K\nu^n$  (Espinoza et al. (2011), and references therein), where  $K$  is a positive constant depending on the moment of inertia and the magnetic dipole moment of the neutron star, and  $n$  is the braking index derived with  $n = \nu\ddot{\nu}/\dot{\nu}^2$ , which is related to the physics mechanism slowing down the pulsar rotation, and  $n = 3$  is expected if the spin-down is dominated by pure magnetodipole radiation (Manchester & Taylor 1977). Currently, only twelve pulsars have reliably measured braking indices because the timing noise and stochastic variations of the pulsar spin-down make accurate determinations of the braking index very difficult. The measured  $n$  values are in the range 0.9–3.15 (Espinoza et al. 2011, 2017; Archibald et al. 2016; Clark et al. 2016),

Some pulsars show rotation state transition behaviors. The emission of PSR B1931+24 switches on and off periodically, and the transition could finish in 10 seconds (Kramer et al. 2006). Lyne et al. (2010) reported that some pulsars show correlation between the variation of spin-down rate  $|\dot{\nu}|$  and pulse profile change. PSR J2021+4026 is the first variable  $\gamma$ -ray pulsar, whose  $\gamma$ -ray flux and pulse profile change with  $|\dot{\nu}|$  variations (Allafort et al. 2013; Zhao et al. 2017; Takata et al. 2020). PSR B0540–69 is the first young pulsar detected to have spin-down rate transition. It results in a delayed brightening of its pulsar wind nebula (Ge et al. 2019). However, the pulsed X-ray flux and profile of PSR B0540–69 show no variations in this process different from the previous reported pulsars. It is believed that these state transition behaviors are probably induced by the changes of the magnetosphere, though the detailed mechanism is unclear.

PSR J1124–5916 is associated with supernova remnant G292.0+1.8 (Camilo et al. 2002; Hughes et al. 2003). It has a characteristic age ( $\tau_c$ ) of 2900 yr and a spin-down luminosity  $\dot{E}$  of  $1.2 \times 10^{37}$  erg s $^{-1}$ , making it the sixth youngest and the sixth most energetic pulsar detected so far. The pulse signals from this object have been detected in the radio, X-ray and  $\gamma$ -ray bands (Camilo et al. 2002; Hughes et al. 2003; Ray et al. 2011). With the first two years of data collected by the Large Area Telescope (LAT) of the *Fermi* Gamma-ray Space Telescope (*Fermi*), the braking index of PSR J1124–5916 is determined as  $-3.78$  (Ray et al. 2011). Here we report the discovery of state transitions of this pulsar and the new measurement of its braking index, using the twelve-year long *Fermi*-LAT observations and the previous results from Camilo et al. (2002), Hughes et al. (2003) and Abdo et al. (2010b).

## 2. Observations and Timing Analysis

LAT is the main instrument of *Fermi*, which could obtain the directional measurement, energy measurement for  $\gamma$ -rays, and background discrimination, respectively (Atwood et al. 2009). The energy range of LAT is from 20 MeV to 300 GeV and the effective area is  $\sim 8000 \text{ cm}^2$ . As *Fermi* can survey the sky frequently with also relatively long exposure, it is suitable to monitor the spin evolution of  $\gamma$ -ray pulsars.

The *Fermi*-LAT observation of PSR J1124–5916 spans from MJD 54763 to 58909. We analyze the data using the standard Fermi Science Tools (v10r0p5). The events are firstly selected using *gtselect* with angular distance less than  $0.5^\circ$ , zenith angle less than  $105^\circ$  and energy range 0.1 to 10 GeV (Abdo et al. 2010a)<sup>1</sup>. Then, the arrival time of every event is corrected to Solar System Barycentre (SSB) using *gtbary* with the solar system ephemerides DE405 and the pulsar position of  $\alpha = 11^{\text{h}}24^{\text{m}}39^{\text{s}}$  and  $\delta = -59^\circ16'19''$  (Ray et al. 2011). Each TOA is accumulated from every 15-day exposure. The detailed procedure could be found in Ge et al. (2019).

In order to show the spin evolution directly, we divide the data set in the whole time range into subsets. The time steps for  $\nu$  and  $\dot{\nu}$  analyses are 60 days and 100 days, respectively. For each subset, the coherent timing analysis is performed using TEMPO2, and the center of the time span is taken as the reference epoch of the timing analysis (Hobbs et al. 2006). Then, the spin evolution of the pulsar in a time interval could be fitted by equation (1).

$$\Phi = \Phi_0 + \nu(t - t_0) + \frac{1}{2}\dot{\nu}(t - t_0)^2 + \frac{1}{6}\ddot{\nu}(t - t_0)^3, \quad (1)$$

where  $\nu$ ,  $\dot{\nu}$  and  $\ddot{\nu}$  are the spin parameters at epoch  $t_0$ . To calculate braking index, equation (2) is utilized to fit the spin evolution covering different time intervals for one state.

$$\nu = \nu_0 + \dot{\nu}(t - t_0) + \frac{1}{2}\ddot{\nu}(t - t_0)^2 + \Delta\nu_{J1} + \Delta\nu_{J2}, \quad (2)$$

where  $\nu_0$ ,  $\dot{\nu}$  and  $\ddot{\nu}$  are the spin parameters at epoch  $t_0$ .  $\Delta\nu_{J1}$  and  $\Delta\nu_{J2}$  are the step values of the spin frequency due to different states.

The timing analysis results obtained by Camilo et al. (2002), Hughes et al. (2003) and Abdo et al. (2010b) are included in this analysis to show the long term evolution of PSR J1124–5916.

---

<sup>1</sup>[https://fermi.gsfc.nasa.gov/ssc/data/analysis/scitools/pulsar\\_analysis\\_tutorial.html](https://fermi.gsfc.nasa.gov/ssc/data/analysis/scitools/pulsar_analysis_tutorial.html)

### 3. Results

The spin evolution between MJD 54600 and 57000 shows different spin-down behaviors after subtracting the long-term evolution trend represented by the quadratic polynomial fitting, as shown in Figure 1 (a) and listed in Table 1. The shape of  $\Delta\dot{\nu}$  is like serration, which means  $\dot{\nu}$  of this pulsar has different values in different epochs. The value of  $\dot{\nu}$  increase on MJD 55183 is  $\Delta\dot{\nu}_u = (191 \pm 9) \times 10^{-15} \text{ Hz s}^{-1}$ , which is consistent with the report by Ray et al. (2011). However,  $\dot{\nu}$  did not experience the exponential recovery process like a normal glitch but remained almost steady until MJD 55803, on which  $\dot{\nu}$  suddenly decreased by  $\Delta\dot{\nu}_d = (-219 \pm 1) \times 10^{-15} \text{ Hz s}^{-1}$  to the value nearly equal to that before MJD 55183. From MJD 56114 to 56398, PSR J1124–5916 behaved similarly, with  $\Delta\dot{\nu}_u = (195 \pm 6) \times 10^{-15} \text{ Hz s}^{-1}$  and  $\Delta\dot{\nu}_d = (-161 \pm 10) \times 10^{-15} \text{ Hz s}^{-1}$ . These sudden changes of  $\dot{\nu}$  are very similar to the spin-down rate transition of PSR B0540–69 though the fractional amplitudes ( $\sim 0.4\%$ ) are about two orders of magnitude smaller (Ge et al. 2019). These variations are also similar to PSR B1931+24 (Kramer et al. 2006) except that the pulse signal does not disappear. From these similarities, we suggest the spin-down state transition of PSR J1124–5916 are probably physically the same as the other pulsar state transitions reported in the literatures (Kramer et al. 2006; Lyne et al. 2010; Marshall et al. 2015; Perera et al. 2015, 2016; Takata et al. 2020). We note here that a glitch happened around MJD 58632, whose parameters are listed in Table 1, but no further discussions on this glitch will be presented in this work.

From Figure 1 we know that the state with higher  $|\dot{\nu}|$  covers much longer time ( $\sim 80\%$ ) than the low  $|\dot{\nu}|$  state, and the former is thus named normal spin-down state. We find that  $|\dot{\nu}|$  in the normal spin-down state decreases linearly with time as represented by the red line in Figure 1 (b). The linear fitting result is listed in Table 1. The two states with lower  $|\dot{\nu}|$  are called the low spin-down state I and the low spin-down state II, respectively. Figure 1 also suggests that there should be some sudden variations before MJD 54600. Particularly, the pulsar might switch to the low spin-down state around MJD 52180 (Camilo et al. 2002), if the main spin-down state between MJD 52105–54600 can be also represented by the red line in Figure 1 (b). The pulsar around MJD 52105 and 53965 might be in normal spin-down state considering the uncertainty of the measured parameters (Hughes et al. 2003; Abdo et al. 2010b).

We checked the  $\gamma$ -ray pulse profiles and fluxes of PSR J1124–5916 in both the normal and low spin-down states to see whether there exist any variations. The two pulse profiles and their differences are plotted in Figure 2. The uniform distribution and the low reduced  $\chi^2$  value (1.29, for 50 d.o.f.) of the differences show that the two profiles are almost identical. The  $\gamma$ -ray flux of PSR J1124–5916 keeps constant whenever in the low spin-down state or

in the normal spin-down state considering the measurement errors<sup>2</sup>. These features are also similar to PSR B0540–69, whose X-ray pulse profile and pulsed flux remain unchanged after state-transition (Ge et al. 2019).

The long time observations also allow us to measure the braking index of PSR J1124–5916. Fitting the results from *Fermi*-LAT, radio and X-ray in MJD 52105 to 58632 by a quadratic polynomial gives a braking index of  $1.8 \pm 0.1$  as listed in Table 1. However, because of the state transition activities, this value might be unreliable. Then, the spin evolution between MJD 56398 and 58632 is selected to calculate the braking index because the pulsar remains in the normal spin-down state in this time interval, and the resulted braking index is  $1.84 \pm 0.06$  (Table 1). Finally, the spin evolution of the whole normal spin-down state is fitted with equation (2) to calculate the braking index and the braking index is  $1.98 \pm 0.04$  (Table 2), which is consistent with the one obtained between MJD 56398 and 58632 within  $2\sigma$ . This makes PSR J1124–5916 the thirteenth pulsar with reliable braking index (Espinoza et al. 2011, 2017; Archibald et al. 2016; Clark et al. 2016). Similarly, the braking indices in low spin-down state I and II could be calculated from the timing solutions listed in Table 2. The braking index in low spin-down state I is  $0.3 \pm 0.1$ , which is smaller than the value in the normal spin-down state and similar to the value of PSR B0540–69 after phase transition (Ge et al. 2019). The braking index in low spin-down state II is  $-2.7 \pm 0.9$ , which is not reliable due to the large timing noise and short time range. Under the assumption that the spin-down is due to the dipole radiation and pulsar wind production, the variations of the braking index imply that the structure of the magnetosphere changes during the spin-down state transition (Ge et al. 2019; Wang et al. 2020).

#### 4. Discussions and Summary

State transitions are very rare events for young pulsars. Besides PSR J1124–5916, only PSR B0540–69 is detected experiencing a state transition with  $|\dot{\nu}|$  increased by 36% in December 2011 within 15 days (Marshall et al. 2015). Although the X-ray luminosity of the pulsar wind surrounding PSR B0540–69 increased gradually up to 30% above the mean pre-transition value, the pulsed X-ray flux and profile remain unchanged (Ge et al. 2019). The spin-down rate increase of PSR B0540–69 is suggested to be the consequence of local changes in the magnetosphere, perhaps in the magnetic pole region, which enhance the pulsar wind production and thus the X-ray brightness of the pulsar wind nebula (Ge et al. 2019). The *Fermi*-LAT observations show that PSR J1124–5916 has transition behaviors similar to PSR

---

<sup>2</sup>[https://fermi.gsfc.nasa.gov/ssc/data/access/lat/8yr\\_catalog/LcPlot2months\\_4FGL\\_v21.pdf](https://fermi.gsfc.nasa.gov/ssc/data/access/lat/8yr_catalog/LcPlot2months_4FGL_v21.pdf)

B0540–69, such as the non-variation of the pulse profile and flux as well as braking index changes. However, both the fractional amplitude of the state transition (0.4%) and the duration of the abnormal spin-down state (about 620 and 280 days) of PSR J1124–5916 are much smaller than those of PSR B0540–69, which are 36% and  $\geq 3000$  days, respectively.

However, state transition behaviors have been detected in a number of radio pulsars and one  $\gamma$ -ray pulsar (Kramer et al. 2006; Lyne et al. 2010; Takata et al. 2020). A common feature of these pulsars is that they are quite old, with characteristic age  $\gtrsim 100$  kyr. PSR B1931+24 shows periodical emission behavior, which could switch off in 10 seconds (Kramer et al. 2006). On the other hand, some pulsars are reported to have gradual  $\dot{\nu}$  changes with timescales of about tens of days to several years (Lyne et al. 2010; Perera et al. 2015, 2016; Takata et al. 2020). The fractional variation amplitude of  $\dot{\nu}$  of PSR J1124–5916 is similar to the amplitudes of some of them. Considering the common features from these pulsars, the state transition of PSR J1124–5916 could be also explained by as the result of changes in the pulsar magnetosphere (Harding et al. 1999; Tong et al. 2013). Ge et al. (2019) suggested that, as the radio emission originates probably in the magnetic pole region and the high energy emission originates from a broader region such as the outer gap (Cheng et al. 1986), the no-change of the  $\gamma$ -ray pulse profile after spin-down state transition does not mean that the radio pulse profile will remain steady. Radio monitoring on PSR J1124–5916 will be helpful to probe the properties of the magnetosphere and the mechanism of spin-down state transition.

Due to the timing noise and stochastic variations in the spin-down evolution, only twelve pulsars have been measured reliable braking indices (Espinoza et al. 2011, 2017; Archibald et al. 2016; Clark et al. 2016). The braking index of PSR J1124–5916 is less than 3 and close to that of PSR B0540–69 before state transition (Espinoza et al. 2011). This means that the spin evolution of PSR J1124–5916 might be dominated by a simple magnetic-dipole radiation and pulsar wind braking scenario (Xu & Qiao 2001; Tong et al. 2013).

In summary, PSR J1124–5916 is the second young pulsar showing state transition behaviors. The  $\dot{\nu}$  evolution of PSR J1124–5916 shows two states named the normal spin-down state and the low spin-down state. The ratio of duration in the normal spin-down state is  $\sim 80\%$  and in the rest of time it switches to the low spin-down state twice. However, the  $\gamma$ -ray pulse profile and flux did not show variations after state transition within the uncertainty of the measurements. Finally, we measured its braking index as  $1.98 \pm 0.04$  utilizing the observation of whole normal spin-down state.

We thank F. F. Kou for helpful discussions on the braking index of pulsars. This

work is supported by the National Key R&D Program of China (2016YFA0400800) and the National Natural Science Foundation of China under grants U1938109, U1838201, U1838202, 11873080, 11903001, U1838104 and U1838101. We acknowledge the use of the public data from the *Fermi* data archive.

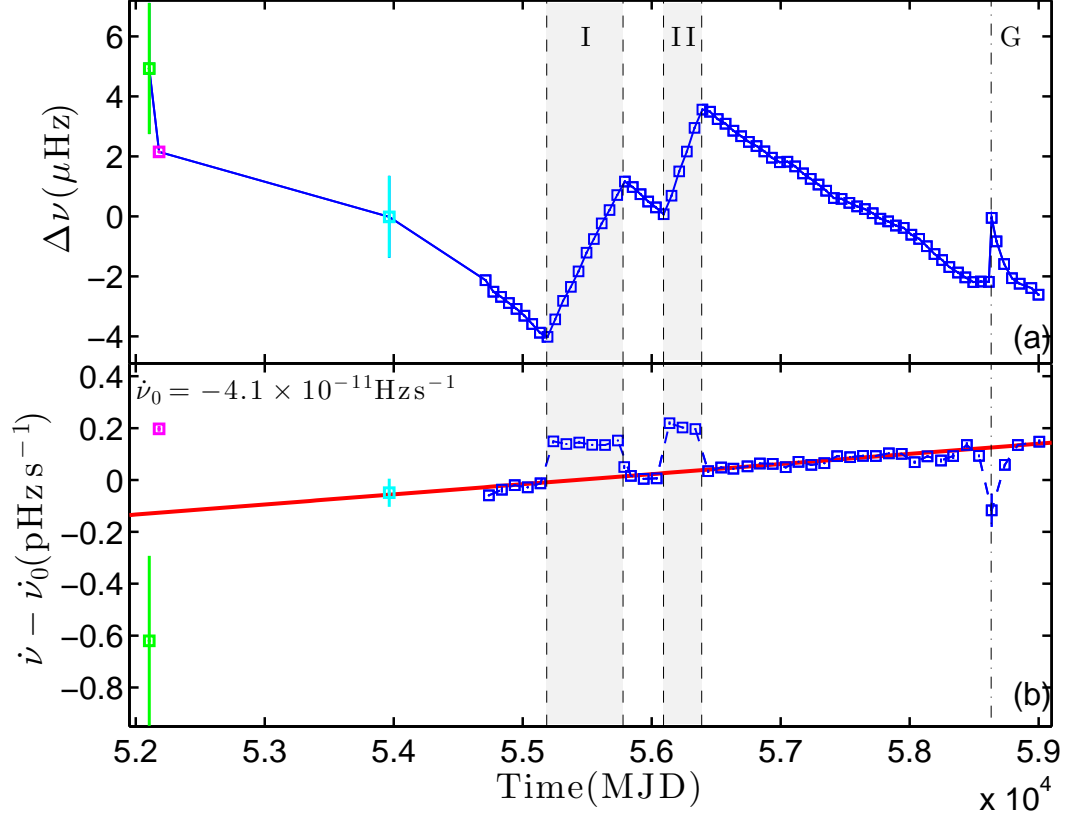


Fig. 1.— The spin frequency evolution of PSR J1124–5916. Panel (a): The spin evolution with the quadratic polynomial fitting result listed in Table 1 subtracted. The green, purple and cyan square points are taken from Hughes et al. (2003), Camilo et al. (2002) and Abdo et al. (2010b), respectively. Panel (b): The  $\dot{\nu}$  evolution, where  $\dot{\nu}_0 = -4.1 \times 10^{-11} \text{ Hz s}^{-1}$ . The red line represents the evolution of  $\dot{\nu}$  obtained by fitting to the  $\nu$  values of whole normal spin-down state with equation (2), and the fitting parameters are listed in Table 2. The value of  $\dot{\nu}$  at MJD 53965 is derived from the frequency at this epoch and the first frequency result on MJD 54738 by *Fermi*-LAT. The four vertical dashed lines represent the start time and stop time of state transitions. The two gray belts represent the low spin-down states. The glitch epoch is marked by the dot-dashed line.



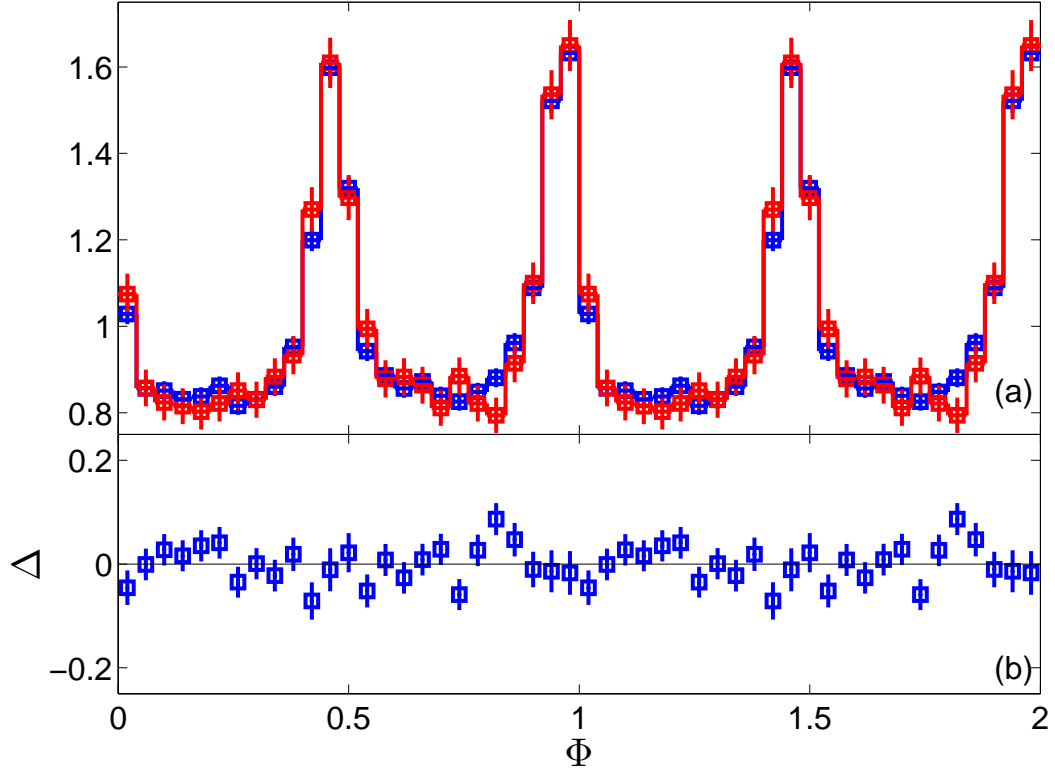


Fig. 2.— The pulse profiles of PSR J1124-5916. Panel (a): The red and blue lines represent the normalized profiles obtained from the low spin-down states and the normal spin-down state. The normalized profile is obtained from the preliminary profile divided by its mean value. Panel (b): The differences between two pulse profiles.

Table 1: Timing parameters of PSR J1124–5916.

Parameters	Value
R.A.	11:24:39.0
Decl.	-59:16:19
Epoch(MJD)	55000
Time range	52105–58632
$\nu$ (Hz)	7.3802155(4)
$\dot{\nu}(10^{-11} \text{ Hz s}^{-1})$	-4.0978(3)
$\ddot{\nu}(10^{-22} \text{ Hz s}^{-2})$	4.16(24)
$n$	1.8(1)
Time range	56398–58632
Epoch(MJD)	57500
$\nu$ (Hz)	7.37137457(3)
$\dot{\nu}(10^{-11} \text{ Hz s}^{-1})$	-4.09186(3)
$\ddot{\nu}(10^{-22} \text{ Hz s}^{-2})$	4.18(12)
$n$	1.84(6)
Glitch	
Time range	58632–58999
Epoch(MJD)	58632(10)
$\Delta\nu$ ( $10^{-6} \text{ Hz}$ )	0.18(17)
$\Delta\nu/\nu$ ( $10^{-9}$ )	25(21)
$\Delta\dot{\nu}(10^{-15} \text{ Hz s}^{-1})$	-3.1(5)
$\Delta\dot{\nu}/\dot{\nu}(10^{-3})$	0.77(13)
$\Delta\nu_d(10^{-6} \text{ Hz})$	2.1(2)
$\tau(\text{day})$	87(7)

The confidence interval is 68.3%.

Table 2: The state transition parameters of PSR J1124–5916.

Parameters	Value
Normal spin-down state	
Epoch(MJD)	56600
Time range	54600–55183, 55803–56114, 56398–58632
$\nu(10^{-6} \text{ Hz})$	7.37455773(3)
$\dot{\nu}(10^{-11} \text{ Hz s}^{-1})$	-4.09537(8)
$\ddot{\nu}(10^{-22} \text{ Hz s}^{-2})$	4.50(9)
$\Delta\nu_{J1}(10^{-6} \text{ Hz})$	-11.2(2)
$\Delta\nu_{J2}(10^{-6} \text{ Hz})$	4.3(1)
$n$	1.98(4)
Low spin-down state I	
Time range	55183(5)-55803(5)
Epoch(MJD)	55600
$\nu(\text{Hz})$	7.3780914669(9)
$\dot{\nu}(10^{-11} \text{ Hz s}^{-1})$	-4.08593(1)
$\ddot{\nu}(10^{-22} \text{ Hz s}^{-2})$	0.76(21)
$n$	0.3(1)
$\Delta\nu_u(10^{-9} \text{ Hz})$	-27(10)
$\Delta\dot{\nu}_u(10^{-15} \text{ Hz s}^{-1})$	191(9)
$\Delta\nu_d(10^{-9} \text{ Hz})$	-252(8)
$\Delta\dot{\nu}_d(10^{-15} \text{ Hz s}^{-1})$	-219(1)
Low spin-down state II	
Time range	56114(5)-56398(11)
Epoch(MJD)	56250
$\nu(\text{Hz})$	7.375794274(4)
$\dot{\nu}(10^{-11} \text{ Hz s}^{-1})$	-4.07937(4)
$\ddot{\nu}(10^{-22} \text{ Hz s}^{-2})$	-6(2)
$n$	-2.7(9)
$\Delta\nu_u(10^{-9} \text{ Hz})$	363(9)
$\Delta\dot{\nu}_u(10^{-15} \text{ Hz s}^{-1})$	195(6)
$\Delta\nu_d(10^{-9} \text{ Hz})$	1(11)
$\Delta\dot{\nu}_d(10^{-15} \text{ Hz s}^{-1})$	-161(10)

The confidence interval is 68.3%.

## REFERENCES

- Abdo, A. A., Ackermann, M., Ajello, M., et al., 2010, *ApJ*, 708, 1254
- Abdo, A. A., et al. 2010, *ApJS*, 187, 460
- Allafort, A., Baldini, L., Ballet, J., et al. 2013, *ApJ*, 777, L2
- Archibald, R. F., Gotthelf, E.V., Ferdman, R.D., et al. 2016, *ApJ*, 819, L16
- Atwood, W. B., Abdo, A. A., Ackermann, M., et al. 2009, *ApJ*, 697, 1071
- Camilo, F., Manchester, R. N., Gaensler, B. M., et al. 2002, *ApJ*, 567, L71
- Cheng, K. S., Ho, C., & Ruderman, M. 1986, *ApJ*, 300, 500
- Clark, C. J., Pletsch, H.J., Wu, J., et al. 2016, *ApJ*, 832, L15
- Espinoza, C. M., Lyne, A. G., Kramer, M., et al. 2011, *ApJ*, 741, L13
- Espinoza, C. M., Lyne, A. G., & Stappers, B. W. 2017, *MNRAS*, 466, 147
- Ge, M.Y., Lu, F. J., Yan, L. L., Weng, S. S., et al., 2019, *NatAs*, 2, 1122
- Harding, A. K., Contopoulos, I., & Kazanas, D. 1999, *ApJ*, 525, L125
- Hobbs, G. B., Edwards, R. T. & Manchester, R. N, 2006, *MNRAS*, 369, 655
- Hughes, J. P., Slane, P. O., Park, S., et al. 2003, *ApJ*, 591, L139
- Kim, M., & An, H. 2019, *Journal of Korean Astronomical Society*, 52, 41
- Kramer, M., Lyne, A. G., O’Brien, J. T., et al. 2006, *Science*, 312, 549
- Kou, F.-F., Ou, Z.-W., & Tong, H. 2016, *Research in Astronomy and Astrophysics*, 16, 79
- Lyne, A. G., Pritchard, R. S., & Graham Smith, F. 1993, *MNRAS*, 265, 1003
- Lyne, A., Hobbs, G., Kramer, M., et al. 2010, *Science*, 329, 408
- Manchester, R. N., & Taylor, J. H. 1977, San Francisco : W. H. Freeman
- Marshall, F. E., Guillemot, L., Harding, A. K., et al. 2015, *ApJ*, 807, L27
- Marshall, F. E., Guillemot, L., Harding, A. K., et al. 2016, *ApJ*, 827, L39
- Perera, B. B. P., Stappers, B. W., Weltevrede, P., et al. 2015, *MNRAS*, 446, 1380

- Perera, B. B. P., Stappers, B. W., Weltevrede, P., et al. 2016, MNRAS, 455, 1071
- Ray, P. S., Kerr, M., Parent, D., et al. 2011, ApJS, 194, 17
- Takata, J., Wang, H. H., Lin, L. C. C., et al. 2020, ApJ, 890, 16
- Tong, H., Xu, R. X., Song, L. M., et al. 2013, ApJ, 768, 144
- Wang, L. J., Ge, M. Y., Wang, J. S., et al. 2020, MNRAS, doi:10.1093/mnras/staa884
- Xu, R. X., & Qiao, G. J. 2001, ApJ, 561, L85
- Zhao, J., Ng, C. W., Lin, L. C. C., et al. 2017, ApJ, 842, 53